Broadly Tunable Subterahertz Emission from Internal Branches of the Current-Voltage Characteristics of Superconducting Bi2Sr2CaCu208+δ Single Crystals

doi: 10.1103/PhysRevLett.108.107006

Broadly Tunable Subterahertz Emission from Internal Branches of the Current-Voltage Characteristics of Superconducting $Bi_2Sr_2CaCu_2O_{8+\delta}$ Single Crystals

Manabu Tsujimoto,[1,2,3] Takashi Yamamoto,[1,2,3,*] Kaveh Delfanazari,[1,2,3] Ryo Nakayama,[1,2,3] Takeo Kitamura,[1,2,3] Masashi Sawamura,[1,2,3] Takanari Kashiwagi,[1,2,3] Hidetoshi Minami,[1,2,3] Masashi Tachiki,[1,2,3] Kazuo Kadowaki,[1,2,3,†] and Richard A. Klemm[4]

[1]*Graduate School of Pure and Applied Sciences, University of Tsukuba, 1-1-1, Tennodai, Tsukuba, Ibaraki 305-8573, Japan*
[2]*CREST, Japan Science and Technology Agency, Kawaguchi Center Building, 4-1-8, Honcho, Kawaguchi, Saitama 332-0012, Japan*
[3]*WPI-MANA, 1-1, Namiki, Tsukuba, Ibaraki 305-0044, Japan*
[4]*Department of Physics, University of Central Florida, Orlando, Florida 32816, USA*

(Received 1 September 2011; published 9 March 2012)

Continuous, coherent subterahertz radiation arises when a dc voltage is applied across a stack of the many intrinsic Josephson junctions in a $Bi_2Sr_2CaCu_2O_{8+\delta}$ single crystal. The active junctions produce an equal number of *I-V* characteristic branches. Each branch radiates at a slightly tunable frequency obeying the Josephson relation. The overall output is broadly tunable and nearly independent of heating effects and internal cavity frequencies. Amplification by a surrounding external cavity to allow for the development of a useful high-power source is proposed.

DOI: 10.1103/PhysRevLett.108.107006 PACS numbers: 74.72.−h, 07.57.Hm, 74.50.+r, 85.25.Cp

Continuous, broadly tunable, and coherent sources of electromagnetic (EM) radiation are presently unavailable for frequencies within the ''terahertz gap,'' the 0.3–10 THz range of crucial importance for many applications [1,2]. This gap can be filled by the ac Josephson effect intrinsic to an atomic-scale layered superconductor. Application of a dc voltage V across a single Josephson junction between identical superconductors leads to an ac Josephson current and EM radiation with the same frequency f satisfying the Josephson relation, $f = f_J = (2e/h)V$, where e is the electric charge and h is Planck's constant [3–5]. By using two-dimensional arrays of Josephson junctions between wires of superconducting Nb, coherent radiation was observed when the array was placed parallel to a Nb ground plane [6] that amplified the radiation but did not affect its frequency, which obeyed the Josephson relation. However, the technical problems involved in mass production were formidable.

The layered, high transition temperature T_c superconductor $Bi_2Sr_2CaCu_2O_{8+\delta}$ (Bi-2212) behaves as a stack of intrinsic Josephson junctions (IJJs) [7]. In Bi-2212, each of the junctions is naturally identical, as they are evenly spaced with two junctions per unit cell c-axis edge length of 1.533 nm. Recently, continuous, coherent EM radiation was induced by applying a V across the stack of N IJJs present in small mesas milled out of single crystalline Bi-2212 [8–18]. The mesas typically have thicknesses $d \sim 1$–2 μm and areas that vary from $\sim 4 \times 10^{-9}$ to $\sim 4 \times 10^{-8}$ m^2. The thin mesa shapes were mostly rectangular, but some were square or circular [16]. Since Bi-2212 is extremely anisotropic, behaving for $\boldsymbol{E} \parallel \hat{\boldsymbol{c}}$ as an insulator [7], the three-dimensional mesa structure also behaves as an internal EM cavity, which couples to the nonlinear ac Josephson currents generated in each junction [8–18]. Besides satisfying the Josephson relation for a stack of N IJJs, $f = f_J = (2e/h)V/N$, it was also consistently reported that f locked onto an internal cavity mode frequency $f^c_{m,p}$, where m and p are integers appropriate for the geometry. By neglecting heating effects, for a very thin ($d \ll w \leq \ell$) rectangular cavity of length ℓ and width w, the relevant transverse magnetic $TM^z(m, p)$ modes have frequencies $f^c_{m,p} = (c_0/2n)\sqrt{(m/w)^2 + (p/\ell)^2}$, where c_0 is the speed of light in vacuum and $n = \sqrt{\epsilon} \approx 4.2$ is the index of refraction for $\boldsymbol{E} \parallel \hat{\boldsymbol{c}}$ in Bi-2212 [8–24].

Most workers have thought that the enhancement of the output radiation by the excitation of an internal cavity mode was so strong that the radiation from the ac Josephson current source alone was too weak to observe [8–14,20–22]. However, recently the contributions to the output power from the ac Josephson current source alone and that enhanced by resonance with an internal EM cavity source were found to be comparable in magnitude [15,16,23,24]. This created a great deal of controversy. Here we show clear evidence that the mesas can emit radiation at many frequencies, without strong interaction with an internal EM cavity mode. More importantly, the resulting radiation is tunable over a broad range of frequencies, allowing for the construction of a powerful device that could fill the terahertz gap.

We studied two rectangular mesas, $R1$ and $R2$. $R1$ was prepared by milling a groove into the Bi-2212 substrate, but $R2$ was sandwiched between two Au layers. Further information on $R1$, $R2$, and three other mesas of various shapes are presented in the Supplemental Material [25]. Figure 1(a) is a scanning ion microscope picture of the top of $R1$, with $w = 99.2$–102 μm, $\ell = 137$–140 μm, and groove depth $d \sim 1.3$ μm, before the electrode attachments. $R1$ is $\sim$3% longer and wider at the bottom of the

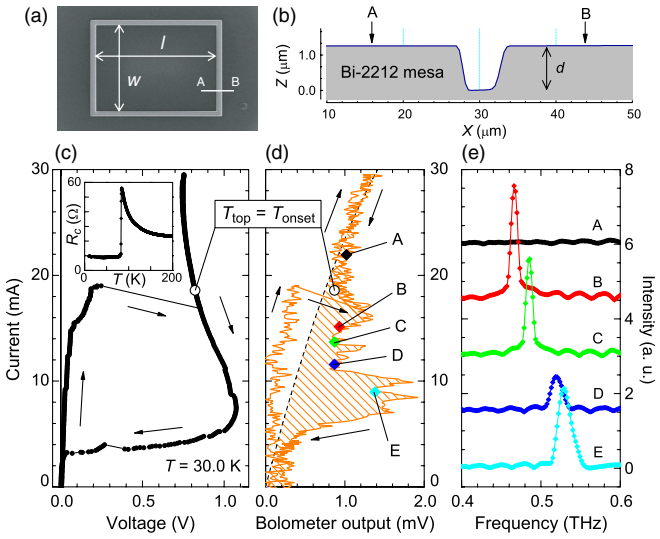

FIG. 1 (color online). $R1$ structure, c-axis resistivity, outermost-branch IVC, emission output, and frequency spectra. (a) Scanning ion microscope image. (b) Atomic force microscope image along A-B in (a). (c) Outer-branch IVC. Inset: $R_c(T)$. (d) Plot of $I(V_{\rm out})$ corresponding to (c). Open circles: $T_{\rm top} = T_{\rm onset} = 84.4$ K. (e) Spectral intensities from points A–E in (d).

groove than at the top. Figure 1(b) is an atomic force microscope scan of the groove profile along the A-B line in Fig. 1(a). From this d value, we estimate the number of IJJs in the stack to be $N_{\rm max} \sim 850$. The hysteresis loop indicated by the arrows in Fig. 1(c) is typical of the outermost branch of the I-V characteristics (IVCs) of an IJJ system. At the largest jump from $V = 0.25$ to 0.85 V, all of the $N_{\rm max}$ junctions switch into the resistive state simultaneously. In the high-V bias region, $R1$ is inevitably Joule heated at a rate of $\sim$16 mW. This huge power dissipation may cause the negative differential resistance between $I = 7$ and 25 mA, since the c-axis quasiparticle resistance R_c has a strong T dependence as shown in the inset in Fig. 1(c). On the return region of the I-V loop where $I \sim 5$ mA, we observed several small steps, indicating that some of the IJJs make the transition from the resistive to the superconducting state.

Figure 1(d) shows the $R1$ radiation output intensity $V_{\rm out}$ generated from I on the same scale as in Fig. 1(c). The dashed curve indicates the expected drift due to thermal radiation from the sample and its holder. Soon after the largest jump in the I-V loop, intense emission of EM waves was clearly observed. Strong spatial variation of the temperature $T_{\rm top}$ over the top mesa surface was previously observed [11,13,14] and was thought to strongly affect the cavity mode-locking condition. We take $T_{\rm top}$ to be the spatial average of the temperature on the mesa top. For $R1$, $T_c = 81.1$ K with a width $\Delta T_c = 6.6$ K. Below $T_{\rm top} = T_{\rm onset} = 84.4$ K, indicated by the open circles in Figs. 1(c) and 1(d), $R1$ makes the transition to the superconducting state, as shown in Fig. 1(d).

Figure 1(e) shows the radiation spectra, offset by 1.5 a.u. for clarity, measured at points A–E in Fig. 1(d), at which all of the $N_{\rm max}$ IJJs are in the resistive state. The narrow and intense peaks in the emission spectra of B–E have maxima varying from 0.47 to 0.53 THz. The detector resolution-limited widths of the B and C peaks are too narrow to arise from synchronization by an internal cavity mode alone and might involve heating effects [13]. Such outermost-branch f tunability of up to 40% was found previously by varying both V and the bath T [13,18,19]. Although the wide f range strongly violates the internal cavity resonance condition $f = f^c_{m,p}$, the Josephson relation for a stack of $N_{\rm max}$ resistive IJJs [13], $f = f_J = (2e/h)V/N_{\rm max}$, is excellently obeyed.

We found that EM emission also occurs at many points in the inner region of the multiply branched IVCs, where $N = 1, 2, \ldots, N_{\rm max}$ is fixed but different for each branch. The synchronization of the N IJJs on a single I-V branch is also not controlled by an internal cavity resonance [26], unlike some predictions [27]. In Figs. 2(a) and 2(b), the radiation frequencies f are plotted as color-scaled symbols on the high-bias regions of the multiply branched I-V structures for $R1$ at 35.0 K and $R2$ at 52.5 K, respectively. The insets show the full IVCs. All of the $R1$ curves in Fig. 2(a) bend backwards with increasing current, indicative of Joule heating [11,13,14,28]. However, $R2$ is less susceptible to heating effects, and its IVCs in Fig. 2(b) are monotonic. The f spectra were obtained at as many (I, V) bias points as possible. At the bias points denoted by open diamonds, no emission was detected.

By repeated measurements of the emission from a particular I-V branch with constant N, we confirmed that f satisfies the ac Josephson relation $f = f_J = (2e/h)V/N$. In Figs. 3(a) and 4(a), we replotted the emission data from

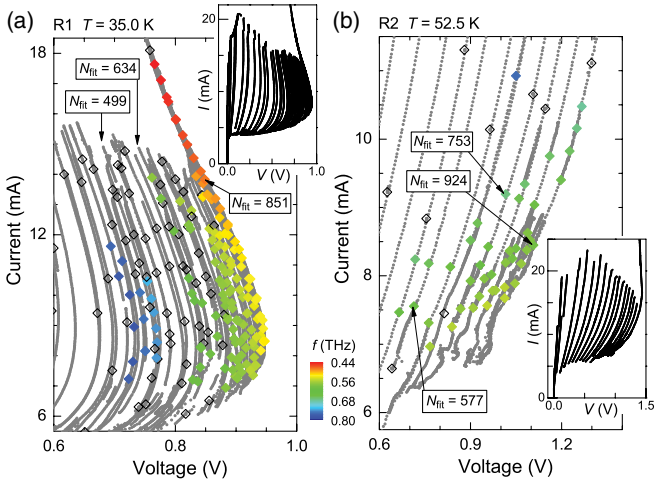

FIG. 2 (color online). Emission from IVC points at the color-coded frequencies was observed at the filled diamonds. No radiation was detected at the open diamonds. Arrows indicate the numbers $N_{\rm fit}$ of resistive junctions from fits to the Josephson relation. (a) $R1$. (b) $R2$. Insets: Full IVCs.

the IVCs of $R1$ and $R2$ shown in Figs. 2(a) and 2(b) in terms of $f(V)$, representing the data from each branch in terms of unique symbols and colors. By fits of the data for a particular branch to the Josephson relation with $N = N_{\rm fit}$, the experimental best-fit value $N_{\rm fit}$ for each emitting branch was determined. Three examples each for $R1$ and $R2$ are, respectively, indicated by the dashed lines in Figs. 3(a) and 4(a) and the arrows in Figs. 2(a) and 2(b). In the insets in Figs. 3(a) and 4(a), the entire emission data from the inner IVC branches of $R1$ and $R2$ are, respectively, plotted as $f(V/N_{\rm fit})$. For both $R1$ and $R2$, the Josephson relation $f = f_J = (2e/h)V/N_{\rm fit}$, represented by each dotted line, is well obeyed.

Since Figs. 3(a) and 4(a) clearly demonstrate that f is slightly tunable on each branch (indicated by a fixed symbol and color), in Figs. 3(b) and 3(c), we, respectively, replotted the data from each $R1$ and $R2$ branch as $f(N_{\rm fit})$. Although for both samples f is tunable as indicated by the vertical bars for each fixed branch number $N_{\rm fit}$, $R1$ and $R2$ display rather different aspects of tunability. The overall tunability of $R1$ and $R2$, which are, respectively, tunable from $0.44\ {\rm THz} \le f \le 0.78\ {\rm THz}$ and from $0.43\ {\rm THz} \le f \le 0.76\ {\rm THz}$, is nearly the same, as indicated in Figs. 3(d) and 4(b). However, for $R1$, this range is primarily due to the f dependence on the I-V branch number, whereas for $R2$, the tunability is greatest on a single branch.

We measured the spectrum for each emitting point in the inner IVC branches of $R1$ and $R2$ and determined its peak intensity as for points B–E on the outer branch of $R1$ shown in Fig. 1(e). In Figs. 3(d) and 4(b), we plotted the peak intensity of the emissions on a logarithmic scale versus f for $R1$ and $R2$, respectively, and $N_{\rm fit}$ is approximately coded with color. The ranges due to mesa profile variations of the respective internal cavity mode frequencies $f^c_{m,p}$ are indicated at the figure tops. For $R1$, no emission was found for $f < 0.40$ THz, excluding the expected cavity resonance frequencies of 0.255 and 0.357 THz corresponding to the $\mathrm{TM}^z(1,0)$ and $\mathrm{TM}^z(0,1)$ modes. Moreover, the spectrum observed in Fig. 3(d) is almost completely unrelated to any of the internal cavity modes. For example, the strongest intensity observed for $f \approx 0.575$ THz, corresponding to $V = 0.894$ V, $I = 9.56$ mA, and $N_{\rm fit} = 753$, is far from the two nearest cavity resonance frequencies. Although the indicated cavity frequency ranges could be shifted to higher frequencies by shorter effective ℓ or d values due to hot spots [13], since $T = 35$ K in each measurement, such shifts could still not explain the broad range of observed frequencies. For $N_{\rm max} = 851$, there are $\sim 4.3 \times 10^{130}$ ways to have $N_{\rm fit}$ of the $N_{\rm max}$ junctions in the resistive state, each of which could in principle lead to a different emission intensity. Hence, multiply cycling through the IVCs led to a large variation in peak intensity at that (I, V) point. The synchronization of the $N_{\rm fit} < N_{\rm max}$ resistive junctions thus occurs independently of the internal cavity mode excitations [26]. More importantly, the emission spectrum in Fig. 3(d) is continuous from $0.44\ {\rm THz} \le f \le 0.78$ THz, except for a gap between 0.66 and 0.73 THz. The gap may be due to some experimental difficulty in accessing the appropriate branches. This widely continuous spectrum independent of

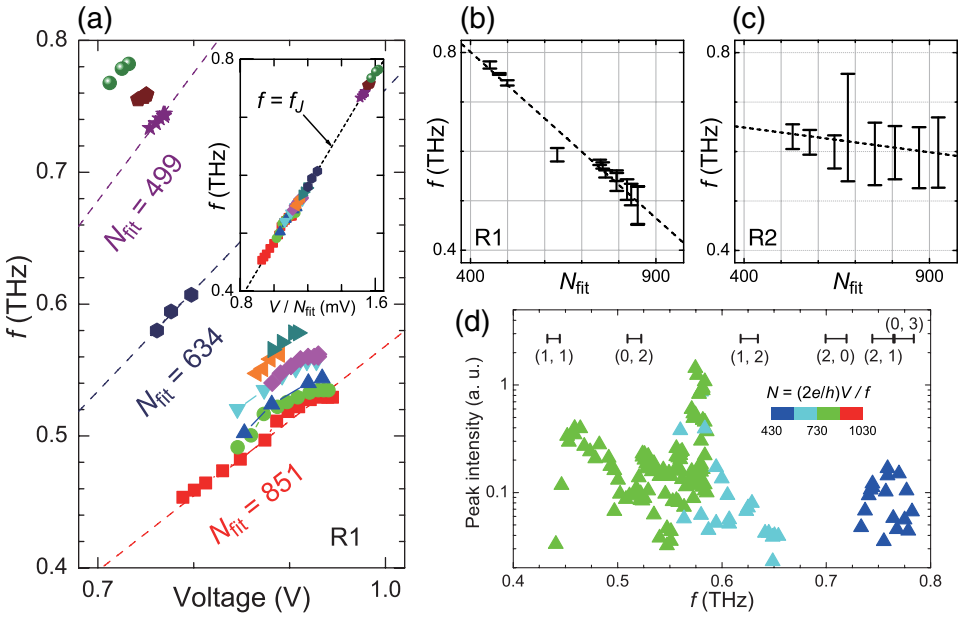

FIG. 3 (color online). Emission frequencies f and intensities from $R1$, and f versus resistive junction numbers $N_{\rm fit}$ for $R1$ and $R2$. (a) $f(V)$ plots for 11 $R1$ IVC branches. Dashed lines: Fits to $f = f_J = (2e/h)V/N_{\rm fit}$. Inset: $f(V/N_{\rm fit})$ plot for all $R1$ data. Dotted line: $f = f_J$. (b),(c) $f(N_{\rm fit})$ ranges for $R1$ and $R2$, with dotted eye guides. (d) Peak intensity on a logarithmic scale versus f for $R1$. Calculated $f^c_{m,p}$ ranges are given at the top. $N_{\rm fit}$ values are color-coded.

internal cavity resonances implies that f is broadly tunable. Figure 3(b) suggests that the f values from lower branch-number emissions could exceed 1 THz. Further tunability might arise from base T variations [13], as discussed in the Supplemental Material [25].

The peak intensity spectrum of $R2$ measured at 52.5 K shown in Fig. 4(b) is also broadly tunable, with emission for 0.43 THz $\leq f \leq$ 0.76 THz and a small gap between 0.67 and 0.75 THz. For $R2$, the f range from 0.43 to ~0.55 THz is below the range of the lowest cavity resonance frequency $f^c_{1,0}$ values. Unlike the peak intensity spectrum of $R1$, the largest intensity at 0.565 THz is close to this $f^c_{1,0}$ range. In this case, the synchronization of the N resistive junctions could be aided by the excitation of this internal cavity mode [26,27].

We measured the full angular dependence of the radiation from $R2$ on the outermost branch at $f = 0.639$ THz, and the results are shown and discussed in the Supplemental Material [25]. Although the observed angular dependence is similar to that expected from the low-Q tail of the TM$^z(1, 0)$ cavity mode excitation, the frequency is far from $f^c_{1,0}$ but could be amplified by excitation of a higher frequency mode, as indicated. We thus determined [15,16,23,24] that the angularly integrated output power at this frequency is ~0.2 μW, somewhat smaller than previously reported [8–19]. In addition, a much larger emission peak intensity, with an estimated overall emission power of 4.8 μW, was found at 0.557 THz, which is much closer to $f^c_{1,0}$. Besides the excitation of the TM$^z(1, 0)$ mode, this strong inner branch emission could have been enhanced by $R2$ being sandwiched between two Au layers [23]. More importantly, the large range in observed f values well below the $f^c_{1,0}$ range is clear evidence that the highly tunable emission itself can occur without excitation of an internal cavity mode.

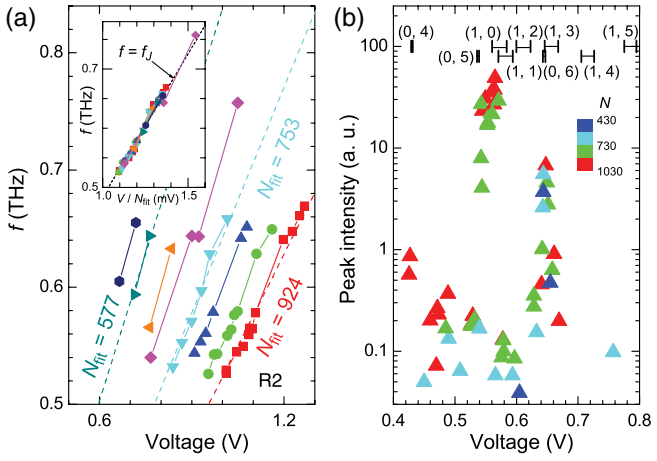

FIG. 4 (color online). Emission frequencies and intensities from $R2$. (a) Plots of $f(V)$ for 8 branches in the $R2$ IVCs. Dashed lines: Fits to $f = f_J = (2e/h)V/N_{fit}$. Inset: Plot of $f(V/N_{fit})$ for all $R2$ data. Dotted line: $f = f_J$. (b) Peak intensity on a logarithmic scale versus f for $R2$. Calculated $f^c_{m,p}$ ranges are given at the top. N_{fit} values are color-coded.

Although $R1$ was prepared by forming a groove into the Bi-2212 substrate, $R2$ stood atop a Au substrate. The heating effects and EM boundary conditions for $R1$ might be significantly different from those for $R2$ [27]. Although the synchronization of the N_{fit} junction emissions from $R2$ is likely to be enhanced by internal cavity resonances [20], synchronization of the N_{fit} emissions from $R1$ could arise from the radiation itself [26] but is more likely to be enhanced by the shunt capacitance in the electrical circuit arising from the nonemitting insulating junctions in the adjacent Bi-2212 substrate [29].

To determine whether the excitation of an internal cavity mode was an essential feature of the coherent radiation obtained from mesas of Bi-2212 under the application of V across the stack of IJJs in the mesa, we examined the inner branches of the IVCs. We found these internal branches to emit radiation over a broad frequency range. Hence, we conclude that the primary source of the intense, coherent subterahertz radiation is the Josephson current and that the internal EM cavity produced by the geometrical shape of the emitting mesa is at best of minor importance and, for one sample, completely irrelevant. Hence, broadband, tunable, continuous coherent radiation can be obtained in the subterahertz f range from Bi-2212 mesas. Since the wavelength in vacuum is $n \approx 4.2$ times longer than in the mesa, we propose that a high-power device can be constructed by surrounding the mesa with an external, tunable high-Q EM cavity [30,31]. By examining yet lower inner branches, it ought to be possible to increase the upper f limit into the 1–10 THz range. Hence, it is now relatively straightforward to produce broadly tunable, continuous, coherent radiation over the range of the terahertz gap.

The authors thank X. Hu, S. Lin, A. Koshelev, M. Matsumoto, T. Koyama, M. Machida, R. Yoshizaki, H. Asai, S. Fukuya, and K. Ivanovic for valuable discussions and Y. Ootuka, T. Hattori, A. Kanda, I. Kakeya, K. Yamaki, and H. Yamaguchi for technical assistance. This work was supported in part by CREST-JST (Japan Science and Technology Agency), WPI (World Premier International Research Center Initiative)-MANA (Materials Nanoarchitectonics) project (NIMS), and Strategic Initiative category (A) at the University of Tsukuba.

*Present address: Quantum Beam Science Directorate, Japan Atomic Energy Agency.
†kadowaki@ims.tsukuba.ac.jp

[1] A. Borak, Science **308**, 638 (2005).
[2] M. Tonouchi, Nature Photon. **1**, 97 (2007).
[3] B. D. Josephson, Phys. Lett. **1**, 251 (1962).
[4] D. N. Langenberg *et al.*, Phys. Rev. Lett. **15**, 294 (1965).
[5] I. K. Yanson, V. M. Svistunov, and I. M. Dmitrenko, Sov. Phys. JETP **21**, 650 (1965).

[6] P. Barbara *et al.*, Phys. Rev. Lett. **82**, 1963 (1999).
[7] R. Kleiner *et al.*, Phys. Rev. Lett. **68**, 2394 (1992).
[8] L. Ozyuzer *et al.*, Science **318**, 1291 (2007).
[9] K. Kadowaki *et al.*, Physica (Amsterdam) **468C**, 634 (2008).
[10] H. Minami *et al.*, Appl. Phys. Lett. **95**, 232511 (2009).
[11] H. B. Wang *et al.*, Phys. Rev. Lett. **102**, 017006 (2009).
[12] L. Ozyuzer *et al.*, Supercond. Sci. Technol. **22**, 114009 (2009).
[13] H. B. Wang *et al.*, Phys. Rev. Lett. **105**, 057002 (2010).
[14] S. Guénon *et al.*, Phys. Rev. B **82**, 214506 (2010).
[15] K. Kadowaki *et al.*, J. Phys. Soc. Jpn. **79**, 023703 (2010).
[16] M. Tsujimoto *et al.*, Phys. Rev. Lett. **105**, 037005 (2010).
[17] K. Yamaki *et al.*, Opt. Express **19**, 3193 (2011).
[18] T. Kashiwagi *et al.*, J. Phys. Soc. Jpn. **80**, 094709 (2011).
[19] T. M. Benseman *et al.*, Phys. Rev. B **84**, 064523 (2011).
[20] L. N. Bulaevskii and A. E. Koshelev, Phys. Rev. Lett. **99**, 057002 (2007).
[21] S. Lin and X. Hu, Phys. Rev. Lett. **100**, 247006 (2008).
[22] M. Tachiki, S. Fukuya, and T. Koyama, Phys. Rev. Lett. **102**, 127002 (2009).
[23] R. A. Klemm and K. Kadowaki, J. Phys. Condens. Matter **22**, 375701 (2010).
[24] R. A. Klemm *et al.*, J. Phys. Condens. Matter **23**, 025701 (2011).
[25] See Supplemental Material at http://link.aps.org/supplemental/10.1103/PhysRevLett.108.107006 for experimental details.
[26] A. Balanov *et al.*, *Synchronization: From Simple to Complex* (Springer, Berlin, 2009).
[27] A. E. Koshelev, Phys. Rev. B **82**, 174512 (2010).
[28] C. Kurter *et al.*, Phys. Rev. B **81**, 224518 (2010).
[29] I. Martin *et al.*, J. Appl. Phys. **108**, 033908 (2010).
[30] E. D. Black, Am. J. Phys. **69**, 79 (2001).
[31] A. H. Clark *et al.*, IEEE J. Quantum Electron. **40**, 878 (2004).